Long-Lived Electronic Coherences in Molecules

Brian Kaufman,[1] Philipp Marquetand,[2] Tamás Rozgonyi,[3] and Thomas Weinacht[1]
[1]Department of Physics and Astronomy, Stony Brook University, Stony Brook, New York 11794-3800, USA
[2]University of Vienna, Faculty of Chemistry, Institute of Theoretical Chemistry, Währinger Strasse 17, 1090 Wien, Austria
[3]Wigner Research Centre for Physics, P.O. Box 49, H-1525 Budapest, Hungary

(Received 18 July 2023; revised 29 September 2023; accepted 1 November 2023; published 26 December 2023)

We demonstrate long-lived electronic coherences in molecules using a combination of measurements with shaped octave spanning ultrafast laser pulses and calculations of the light matter interaction. Our pump-probe measurements prepare and interrogate entangled nuclear-electronic wave packets whose electronic phase remains well defined despite vibrational motion along many degrees of freedom. The experiments and calculations illustrate how coherences between excited states can survive, even when coherence with the ground state is lost, and may have important implications for many areas of attosecond science and photochemistry.

DOI: 10.1103/PhysRevLett.131.263202

The motion of electrons in photoexcited molecules governs many basic light-driven processes in physics, chemistry, and biology. From solar cells to photodissociation and photosynthesis, electronic dynamics play a fundamental role in molecular transformation, and can determine what the final products are [1]. Electronic dynamics can be described in terms of wave packets—coherent superpositions of electronic states, whose evolution is dictated by the relative phase between states [2–4]. While this phase relationship ("electronic coherence") remains well defined in atoms for many cycles [5–7], it is complicated in molecules by the motion of the nuclei, which are entangled with the electrons. The full wave function generally cannot be written as a product of electronic and nuclear wave functions, and the resulting entangled wave function typically leads to a rapid decay in the electronic coherence due to nuclear motion and nonadiabatic dynamics if one integrates over nuclear coordinates. This is clear if one writes the total wave function as a Born-Huang expansion [8]:

$$\Psi(\boldsymbol{r},\boldsymbol{R},t)=\sum_n c_n\chi_n(\boldsymbol{R},t)\psi_n(\boldsymbol{r};\boldsymbol{R}), \tag{1}$$

where $\boldsymbol{r}$ and $\boldsymbol{R}$ represent the electronic and nuclear degrees of freedom, respectively, $\psi_n(\boldsymbol{r};\boldsymbol{R})$ represents the nth electronic eigenstate of the molecule, c_n is the complex amplitude of the nth state, and $\chi_n(\boldsymbol{R},t)$ represents the (normalized) time-dependent nuclear wave function in the nth electronic state [9]. Calculations and measurements over the past two decades have established rather short timescales for decoherence of less than 10 fs [10–16] due to loss of vibrational wave function overlap between $\chi_n(\boldsymbol{R},t)$ and $\chi_m(\boldsymbol{R},t)$ and the different rates of phase advance between electronic states for different $\boldsymbol{R}$ values (dephasing) [10,16,17]. This has led to a significant debate over the role that electronic coherences play in photosynthesis and other natural processes driven by light absorption [18,19]. Here, we demonstrate that while nuclear dynamics in polyatomic molecules can lead to a rapid loss of coherence with the ground state, coherences between excited states can persist for many periods of electronic motion (several hundreds of fs) if the excited-state potential energy surfaces are close to being parallel, since the nuclear motion in the two states is similar, and the vibrational wave function can be roughly factored out of the expression for the total wave function [20,21]. Thus, if one is able to prepare a coherent superposition of such excited electronic states, then the electronic coherence between excited states can be preserved for much longer times, even if one traces over nuclear coordinates in a given measurement. Parallel potential energy surfaces can be found in Rydberg states or for valence states involving lone pair orbitals—situations where the different singly occupied orbitals do not dramatically affect molecular bonding. Figure 1 in the Supplemental Material [22] illustrates such a pair of states for the molecule thiophene. We propose and demonstrate an experiment to create and measure electronic wave packets in polyatomic molecules using ultrabroadband shaped laser pulses and velocity map imaging of the photoelectrons produced by the light-molecule interaction. The measurements are motivated by and interpreted with electronic structure calculations and calculations of the light-matter interaction.

The basic idea is illustrated by Fig. 1, which shows the multiphoton excitation of two excited state potentials that are roughly parallel. The main panel of the figure shows the electronic states as a function of nuclear coordinate $\boldsymbol{R}$. There are four states: the ground state S_0, two displaced but parallel (singlet) excited state potentials S_n and S_m, and a

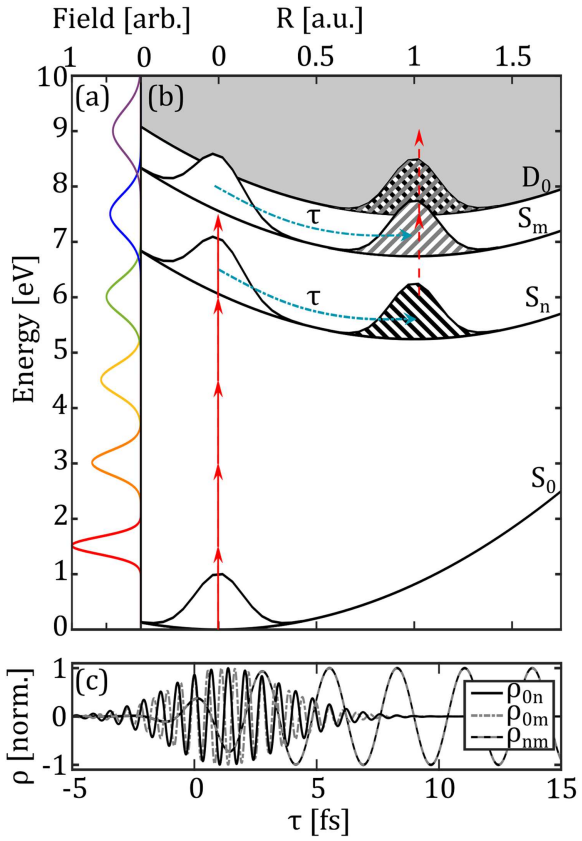

FIG. 1. Illustration of our approach to the creation and detection of long-lived electronic coherences. The main panel, panel (a), shows the creation of an electronic and vibrational wave packet via multiphoton absorption to two roughly parallel excited states of the molecule (S_n and S_m). These wave packets can evolve and are probed by ionization. Interference between the wave packets ionized from S_n and S_m leads to modulations in the ionization yield as a function of pump-probe delay. Panel (a) on the left-hand side illustrates the multiphoton excitation spectrum—i.e., the spectrum of $\epsilon(t)$, and the lower panel, panel (c), shows the coherence between different pairs of states as a function of pump-probe delay.

single displaced (doublet) ionic state D_0. Red arrows highlight coherent multiphoton excitation of these two states—in this case, four and five photon excitations to S_n and S_m, respectively. The left panel of the figure shows the nonlinear spectrum of the pump pulse, illustrating the fact that the nth order spectrum $\epsilon^n(t)$ is $\sqrt{n}$ times broader than the linear spectrum of the laser $\epsilon(t)$, allowing for the possible excitation of multiple electronic states without tuning the laser to a specific multiphoton resonance [35]. These excited states can then be ionized to the same ionic state by two ($S_n \rightarrow D_0$) and one ($S_m \rightarrow D_0$) photons. In a wave-packet picture, the pump pulse launches a wave packet on each excited state, each of which evolves for a time τ to the position of the shaded wave packets before being ionized to the same ionic state, where they can interfere with one another if their coherence is preserved. This interference leads to a modulation in the ionization yield as the phase between the two excited-state wave packets evolves.

The coherence between any pair of states in the total wave function is captured by the off diagonal elements of the density matrix:

$$\rho_{jk}(t) = \int c_j^* c_k e^{i2\pi\nu_{jk}(\boldsymbol{R})t} \chi_j^*(\boldsymbol{R}, t)\chi_k(\boldsymbol{R}, t)d\boldsymbol{R}, \qquad (2)$$

where j and k represent the indices of any two electronic states, c is the amplitude of each state, $h\nu_{jk}(\boldsymbol{R}) = h[\nu_j(\boldsymbol{R}) - \nu_k(\boldsymbol{R})]$ is the coordinate dependent energy difference between the two electronic states, and $\chi_{j,k}(\boldsymbol{R}, t)$ represents the vibrational wave packet. In the bottom panel of Fig. 1, we plot the real part of the three coherence terms ($j, k = 0, n, m$): two ground-excited state coherences, ρ_{0n} and ρ_{0m}, and the excited-excited state coherence, ρ_{nm}. In this example, the ground-excited coherence oscillates rapidly (at the frequency corresponding to the energy difference between states) and then decays within 10 fs as a result of the displacement between the ground and excited state potentials, which leads to dephasing and a decrease in vibrational wave function overlap. For excited states there are slower oscillations due to the smaller energy separation between the potentials. For states with potentials that are not parallel, there would be a similar decay of coherence due to dephasing [$\boldsymbol{R}$ dependence of the phase term in Eq. (2)], the loss of vibrational wave function overlap [product of $\chi_j(\boldsymbol{R}, t)$ and $\chi_k(\boldsymbol{R}, t)$ in Eq. (2)] and internal conversion [decay of c_j and c_k in Eq. (2)] [10,11]. However, in the case of coherences between excited states with parallel potentials, the oscillations can persist for much longer because the parallel potential energy surfaces mitigate dephasing and the loss of vibrational wave function overlap.

In order to create such a coherence, one requires a (potentially nonlinear) excitation spectrum which can span multiple electronic states [36–39]. In order to probe such an electronic coherence, which corresponds to the rapid motion of the electrons moving back and forth across the molecule, one generally requires a probe pulse much shorter than the period of the motion (i.e., subfemtosecond) [39]. However, an alternative approach is to make use of a probe pulse whose phase is well defined with respect to the pump pulse, and is therefore sensitive to the phase of the electronic coherence and motion [40]. If one is able to advance the relative phase between pump and probe pulses with delay at different rates relative to the phase advance of the electronic coherence, then one can effectively "strobe" or slow down the electronic oscillations with respect to pump-probe delay. This can be accomplished with an ultrafast optical pulse shaper by generating a delay dependent phase between the pulses given by $\phi_L(\tau) = 2\pi\tau\nu_L$, where ν_L is a frequency at which the phase between the pulses is "locked." For such a delay-dependent

phase between the pulses, the relative phase between the probe pulse and the electronic coherence evolves with a period given by

$$\tau_b = \frac{1}{\nu_L - \nu_{jk}}. \tag{3}$$

With appropriate choice of ν_L, the beat period (τ_b) can be set to tens of femtoseconds, amenable to probing with few fs pulses.

We use an acousto-optic modulator (AOM) based pulse shaper [41] for compression, characterization, and control of the ultrafast pulses generated by the laser system described in the Appendix. The pulse shaper uses an AOM as a spectral mask $M(\nu)$, to shape the pulse in the frequency domain by placing it in the Fourier plane of a zero dispersion stretcher [42]. The shaped electric field $\epsilon'(\nu)$ is a product of the acoustic mask $M(\nu)$ and the unshaped field $\epsilon(\nu)$: $\epsilon'(\nu) = M(\nu)\epsilon(\nu)$. For the experimental control we use a mask of the form

$$M(\nu) = A\{1 + a\exp[-i2\pi\tau(\nu - \nu_L) + i\phi]\}, \tag{4}$$

where A is the overall amplitude, a is the relative pump-probe amplitude, τ is the pump-probe delay, ν_L is the locking frequency, and ϕ is the relative phase between the pump and probe.

Here, we present multiple measurements of energy integrated photoelectron spectrum (PES) as a function of several mask parameters. First, we measure the PES as a function of the delay, τ, and phase, ϕ between pump and probe pulses. The pump-probe measurements are then carried out for a number of different locking frequencies, ν_L. Figure 2 illustrates the shaped pulses for the pump-probe delay scans with different locking frequencies, in both the frequency and time domains (top left two panels), as well as the same for the phase scans (top right panels). The bottom panels show the associated photoelectron yields as a function of τ and ϕ.

As shown in Fig. 2, the ionization yield depends on pump-probe delay and phase. The pump-probe measurement is a phase-locked delay scan where the frequency is locked at 0.4 PHz—the spectral density remains constant at this frequency (constructive interference) regardless of delay as seen in the top left panel of Fig. 2. This scan shows clear modulations with delay having a period of about 26 fs. The right side of the figure describes a complementary experiment, a delay-locked phase scan, where we vary the relative phase, ϕ in Eq. (4), for a fixed pump-probe delay. As this ϕ changes the carrier with respect to the envelope of the probe pulse, it is similar to a pump-probe measurement with a probe pulse shorter than the oscillation period, where the 2π optical phase corresponds to a delay of one optical period, ~2.5 fs. The bottom right panel of Fig. 2 shows the integrated yield for

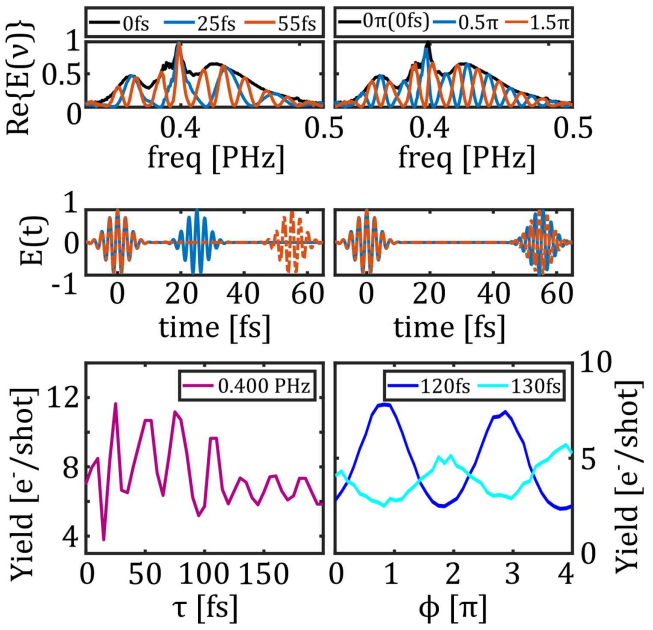

FIG. 2. Combination of the shaped laser field, in time and frequency (top four panels) with the resulting molecular measurements (bottom two panels). The top panels show the measured optical spectrum of the combined pump and probe pulses. The left panel shows pump-probe delays of 0, 25, and 55 fs, with a locking frequency of 0.4 PHz. The top right panel shows the pulses for two different phases (0.5π and 1.5π) at a fixed delay of 55 fs. The middle panels show the simulated fields in the time domain based on measured optical spectra. The bottom left panel shows the photoelectron yield vs pump-probe delay for a locking frequency of 0.4 PHz (phase-locked delay scan), and the bottom right panel shows the yield as a function of phase for two different pump-probe delays (delay-locked phase scan).

two phase scans, at delays of 120 and 130 fs, in dark and light blue, respectively. Note that there is one modulation per 2π phase, which is consistent with a roughly one-photon energy difference between the two states in question. Furthermore, the $\Delta\phi = \pi$ phase difference in the modulations of the yield vs ϕ agrees well with the phase advance one would expect for the difference in delay time, $\Delta\tau$, given by $\Delta\phi = 2\pi(\nu_L - \nu_{nm})\Delta\tau$. The phase-dependent yield suggests that there is a coherent superposition of electronic states (i.e., an electronic coherence) whose ionization yield is sensitive to the phase of the probe pulse. However, it is not immediately clear from the yield vs delay whether the modulations we observe are related to this electronic coherence, or are due to vibrational dynamics.

We performed a series of pump-probe measurements for different locking frequencies to determine whether the modulations in the yield come from electronic or vibrational coherences. In Fig. 3, we show the ionization yield (generated by integrating the PES between 0.4 and 4 eV) as a function of pump-probe delay for five different locking frequencies: 0.382, 0.400, 0.406, 0.414, and 0.422 PHz. For visual clarity, the yield is normalized and offset such

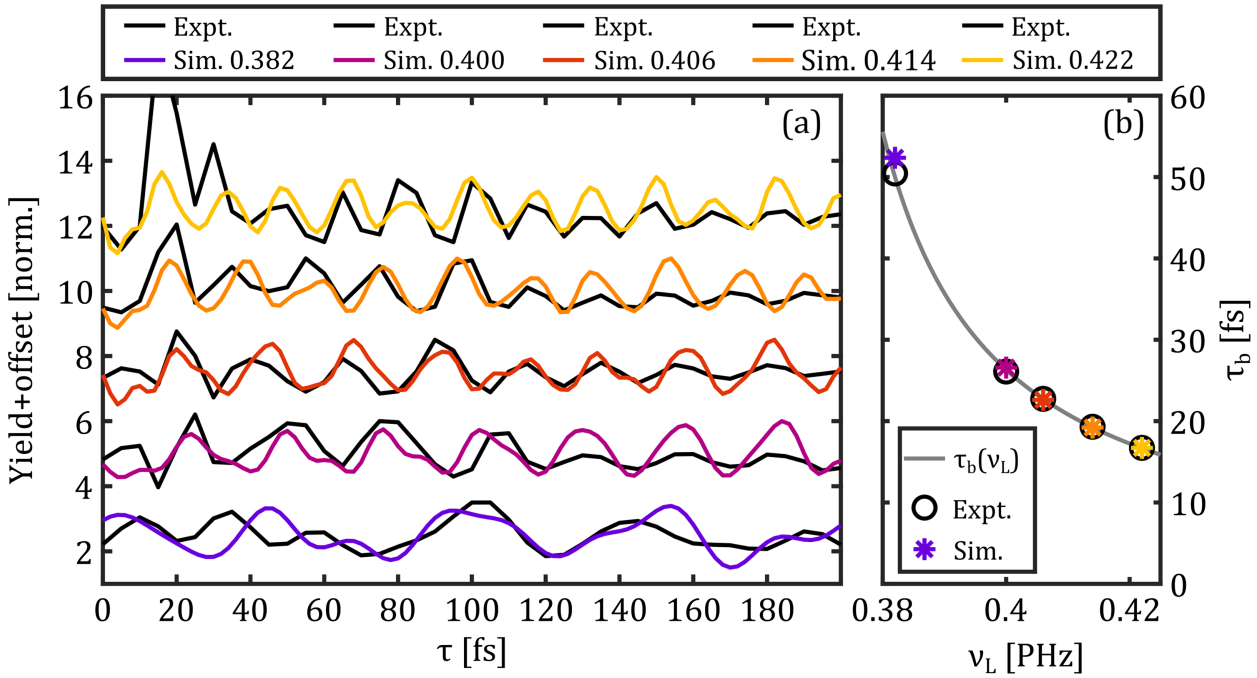

FIG. 3. Panel (a): Photoelectron yield as a function of pump-probe delay for five locking frequencies: 0.382, 0.400, 0.406, 0.414, and 0.422 PHz. The experimental measurements (Expt) are plotted in black and overlaid with the colored simulations (Sim) at the same locking frequency. For visual clarity each curve is normalized and given an arbitrary offset ($+2.5 \times n$). Simulation results were low pass filtered to remove fast oscillations arising from ground to excited state coherences—see Supplemental Material [22], Fig. 4 for details. Panel (b): Comparison of Eq. (3) with the calculated and measured modulation period of the yield as a function of pump-probe delay for different locking frequencies.

that the lowest yield is for the lowest locking frequency. Each of the measurements show modulations in the ionization yield with pump-probe delay persisting beyond 200 fs. The fact that the modulation period varies with locking frequency clearly demonstrates that the modulations are due to the electronic coherence and not a vibrational one. In order to reinforce this point, we compare the measurements with calculations of the observable. The black curves show the experimentally measured yield and the overlaid colored curves show the results of the quantum-dynamics simulations described below.

The quantum-dynamics calculations, described in the Appendix, solved the time-dependent Schrödinger equation (TDSE) for a model system that includes multiphoton coupling, a discretized ionization continuum, and vibrational dynamics in one dimension. The states consist of the neutral ground state, labeled S_0, two singlet excited states, S_n and S_m, and one doublet cationic state, D_0 in line with the cartoon shown in Fig. 1. Given the one-dimensional nature of our model, the fact that the experiments averaged over all molecular orientations, and a number of other complications, the goal of our quantum calculations was not to solve the TDSE for molecular thiophene under the exact experimental conditions, but rather to provide a simple model that aims to capture the essential features of the physical process behind the measurements.

The agreement between the measurements and the four-state, one-dimensional quantum-dynamics calculations is remarkable given the simplicity of the model. In particular, the fact that the modulation period varies with locking frequency in both the measurements and simulations in the same way indicates that they are not due to vibrational dynamics but rather electronic dynamics that persist despite the fact that our measurements of the photoelectron yield trace over vibrational coordinates. The main discrepancy is in the variation of the depth of modulation in the measurements, which is not reflected in the calculations. We argue that this variation in the depth of modulation comes from the dephasing and variation in the multidimensional vibrational wave function overlap, as shown in Eq. (2).

A key test of our interpretation is whether the modulation period in the measured yield for each locking frequency, ν_L can be described by Eq. (3) for a single resonance frequency, ν_{nm}. We therefore fit a cosine curve to each of the curves in Fig. 3 and extract the modulation period. In the right panel of Fig. 3, we plot this period as a function of locking frequency. The black circles show the experimental periods and the colored stars show the simulation periods. These data points are overlaid on a plot of Eq. (3), showing excellent agreement between experiment and simulation. Fitting the experimental data to Eq. (3), allows us to determine the resonance frequency, ν_{nm}, between the

electronic states in the coherent superposition. This resonance frequency roughly matches the separation between the highlighted states in Supplemental Material, Fig. 1 [22].

As a check of our interpretation and to test whether the idea can be reproduced in another molecule, we carried out similar measurements for the molecule furan, which has a very similar structure to thiophene, with the sulfur atom replaced by an oxygen. Figure 2 in the Supplemental Material [22] compares the measurements for thiophene with furan out to pump-probe delays of 500 fs, demonstrating similar long-lived electronic coherences in the two molecules.

In conclusion, we demonstrate long-lived (hundreds of fs) electronic coherences (superpositions of electronic states) in a molecular system with parallel potentials, as one could expect from, e.g., lone pair states and Rydberg states. The parallel potentials allow one to roughly factor the generally entangled total wave function into electronic and nuclear parts, leading to the survival of an electronic coherence over many periods. These measurements are relevant to the role of electronic coherences in chemistry and biology, and motivate further work to determine the extent to which electronic coherences can survive and drive chemical changes in larger molecules.

This work was supported by National Science Foundation under Grant No. 2110376. T. R. acknowledges support from the National Research, Development and Innovation Fund of Hungary under Grants No. 2018-1.2.1-NKP-2018-00012 and No. SNN 135636.

Appendix: Experimental and calculational details.—Our measurements make use of an amplified Ti:sapphire laser system generating 1 mJ transform limited pulses of 30 fs duration, centered at a wavelength of 780 nm, and operating at a 1 kHz repetition rate. The pulses are spectrally broadened using self-phase modulation in a 2.1 m stretched-hollow core fiber (S-HCF) filled with 600 Torr of ultrahigh purity argon gas. The S-HCF produces a slightly blueshifted spectrum (central wavelength of 750 nm), extending from 600 to 900 nm [43–45]. The broadened spectrum is compressed to near transform limit, 7 fs, using a phase mask modeled by a Taylor-series expansion up to fourth order dispersion combined with the residual reconstructed phase from a pulse-shaper-assisted dispersion scan (PS-DSCAN) [45]. This is then characterized using pulse-shaper-assisted, second harmonic generation collinear frequency resolved optical gating (PS-CFROG) [46,47]. The shaped pulses are focused in an effusive molecular beam inside a vacuum chamber with a base pressure of $\sim 10^{-10}$ Torr, raising the working pressure to about $\sim 10^{-6}$ Torr. The molecules are ionized by the laser pulses, with peak intensities of up to $\sim 10^{13}$ W/cm^2. The electrons generated by ionization are velocity map imaged to a dual-stack microchannel plate (MCP) and phosphor screen detector using an electrostatic lens. The light emitted by the phosphor screen at each position is recorded by a CMOS camera. The camera measurements are inverse Abel transformed to reconstruct the three-dimensional momentum distribution of the outgoing electrons and the photoelectron spectrum (PES).

The calculations use grid-based one-dimensional wave-packet dynamics simulations, where the potentials are harmonic and inspired by the electronic structure calculations shown in Supplemental Material Fig. 1 [22]. The excited states are coupled to the ground state S_0 by multiphoton transitions. The formulas for the multiphoton couplings are derived via adiabatic elimination [48–50], where the effect of off-resonant states that mediate the multiphoton transitions is reproduced in the form of Rabi frequencies Ω. The state energies and vibrational frequencies used in the model are inspired by our electronic structure calculations for thiophene, which formed the basis of Fig. 1 in the Supplemental Material [22]. The coupling parameters are loosely based on multiphoton absorption calculations carried out in earlier work [35], and are given in Table I and II in Ref. [22].

The laser-pulse parameters in the numerical model are based on the experimental ones: we used a central frequency, $\nu_0 = 362$ THz, peak intensity of 12 TW/cm^2 and an intensity envelope with a full-width at half maximum of 7 fs. As in the experiment, the pulse is shaped by applying Eq. (4) to the pulse in the frequency domain.

Details of the equations behind the model are described in Supplemental Material [22] and Refs. [51,52].

Both the measurements and calculations were carried out for a variety of pump and probe intensities [different a values in Eq. (4)]. The measurements and calculations shown in Fig. 3 are for pump and probe pulse intensities of 6 and 12 TW/cm^2, respectively. Measurements and calculations for slightly lower or higher intensities ($\pm 20\%$) showed similar yields vs pump-probe delay. Interestingly, the measurements show similar modulations in both regimes of strong-pump weak-probe and vice versa, as shown in Fig. 3 of the Supplemental Material [22]. Comparing the two suggests that there are more than just two electronic states involved in the dynamics, and the intensity of the pump and probe pulses can influence their relative importance.

[1] H. J. Wörner, C. A. Arrell, N. Banerji, A. Cannizzo, M. Chergui, A. K. Das, P. Hamm, U. Keller, P. M. Kraus, E. Liberatore *et al.*, Struct. Dyn. **4**, 061508 (2017).

[2] A. S. Folorunso, A. Bruner, F. m. c. Mauger, K. A. Hamer, S. Hernandez, R. R. Jones, L. F. DiMauro, M. B. Gaarde, K. J. Schafer, and K. Lopata, Phys. Rev. Lett. **126**, 133002 (2021).

[3] S. Haessler, J. Caillat, W. Boutu, C. Giovanetti-Teixeira, T. Ruchon, T. Auguste, Z. Diveki, P. Breger, A. Maquet, B. Carré *et al.*, Nat. Phys. **6**, 200 (2010).

[4] T. Okino, Y. Furukawa, Y. Nabekawa, S. Miyabe, A. Amani Eilanlou, E. J. Takahashi, K. Yamanouchi, and K. Midorikawa, Sci. Adv. **1**, e1500356 (2015).

[5] T. C. Weinacht, J. Ahn, and P. H. Bucksbaum, Phys. Rev. Lett. **80**, 5508 (1998).

[6] J. A. Yeazell, M. Mallalieu, and C. R. Stroud, Phys. Rev. Lett. **64**, 2007 (1990).

[7] H. Maeda and T. F. Gallagher, Phys. Rev. Lett. **92**, 133004 (2004).

[8] M. Born and K. Huang, Oxford University Press, Oxford **2**, 1954 (1985).

[9] We note that this expansion is slightly different from the standard Born-Huang expansion, for which the c_n coefficient is included in the vibrational wave function $\chi_n(\boldsymbol{R}, t)$. We have separated c_n out here since it allows us to use normalized vibrational wave functions and separate the parts of the wave function that are laser dependent from those that are not.

[10] C. Arnold, O. Vendrell, and R. Santra, Phys. Rev. A **95**, 033425 (2017).

[11] G. Halász, A. Perveaux, B. Lasorne, M. Robb, F. Gatti, and Á. Vibók, Phys. Rev. A **88** (2013).

[12] I. Franco, M. Shapiro, and P. Brumer, J. Chem. Phys. **128**, 244905 (2008).

[13] A. Scheidegger, J. Vaníček, and N. V. Golubev, J. Chem. Phys. **156**, 034104 (2022).

[14] H. Hwang and P. J. Rossky, J. Phys. Chem. B **108**, 6723 (2004).

[15] H. Kamisaka, S. V. Kilina, K. Yamashita, and O. V. Prezhdo, Nano Lett. **6**, 2295 (2006).

[16] M. Vacher, M. J. Bearpark, M. A. Robb, and J. a. P. Malhado, Phys. Rev. Lett. **118**, 083001 (2017).

[17] M. Vacher, L. Steinberg, A. J. Jenkins, M. J. Bearpark, and M. A. Robb, Phys. Rev. A **92**, 040502(R) (2015).

[18] H.-G. Duan, V. I. Prokhorenko, R. J. Cogdell, K. Ashraf, A. L. Stevens, M. Thorwart, and R. D. Miller, Proc. Natl. Acad. Sci. U.S.A. **114**, 8493 (2017).

[19] M. Maiuri, E. E. Ostroumov, R. G. Saer, R. E. Blankenship, and G. D. Scholes, Nat. Chem. **10**, 177 (2018).

[20] V. Despré, N. V. Golubev, and A. I. Kuleff, Phys. Rev. Lett. **121**, 203002 (2018).

[21] A. Csehi, P. Badankó, G. J. Halasz, Á. Vibók, and B. Lasorne, J. Phys. B **53**, 184005 (2020).

[22] See Supplemental Material at http://link.aps.org/supplemental/10.1103/PhysRevLett.131.263202 for additional experimental and theoretical details including *ab initio* calculations of potential curves along normal modes, wave packet dynamics, long delays experimentally measured for two heterocyclic aromatics, weak-pump–strong-probe and strong-pump–weak-probe experimental measurements, Fourier filtered simulated measurements, and experimental reproducibility. The Supplemental Material includes Refs. [23–34].

[23] M. J. Frisch, G. W. Trucks, H. B. Schlegel, G. E. Scuseria, M. A. Robb, J. R. Cheeseman, G. Scalmani, V. Barone, B. Mennucci, G. A. Petersson *et al.*, GAUSSIAN 2009, Gaussian Inc., Wallingford, CT, 2009.

[24] P. J. Stephens, F. J. Devlin, C. F. Chabalowski, and M. J. Frisch, J. Phys. Chem. **98**, 11623 (1994).

[25] K. A. Peterson, D. Figgen, E. Goll, H. Stoll, and M. Dolg, J. Chem. Phys. **119**, 11113 (2003).

[26] J. Finley, P.-A. Malmqvist, B. O. Roos, and L. Serrano-Andrés, Chem. Phys. Lett. **288**, 299 (1998).

[27] K. Andersson, P.-A. Malmqvist, and B. O. Roos, J. Chem. Phys. **96**, 1218 (1992).

[28] I. F. Galván *et al.*, J. Chem. Theory Comput. **15**, 5925 (2019).

[29] M. Reiher, Theor. Chem. Acc. **116**, 241 (2006).

[30] P.-O. Widmark, P.-A. Malmqvist, and B. O. Roos, Theor. Chim. Acta **77**, 291 (1990).

[31] B. O. Roos, R. Lindh, P.-A. Malmqvist, V. Veryazov, and P.-O. Widmark, J. Phys. Chem. A **108**, 2851 (2004).

[32] C. Trallero-Herrero, D. Cardoza, T. C. Weinacht, and J. L. Cohen, Phys. Rev. A **71**, 013423 (2005).

[33] M. Seel and W. Domcke, J. Chem. Phys. **95**, 7806 (1991).

[34] T. Rozgonyi, A. Glass, and T. Feurer, J. Appl. Phys. **88**, 2936 (2000).

[35] B. Kaufman, P. Marquetand, T. Weinacht, and T. Rozgonyi, Phys. Rev. A **106**, 013111 (2022).

[36] F. Calegari, D. Ayuso, A. Trabattoni, L. Belshaw, S. De Camillis, S. Anumula, F. Frassetto, L. Poletto, A. Palacios, P. Decleva *et al.*, Science **346**, 336 (2014).

[37] N. Rohringer and R. Santra, Phys. Rev. A **79**, 053402 (2009).

[38] D. Schwickert, M. Ruberti, P. Kolorenč, S. Usenko, A. Przystawik, K. Baev, I. Baev, M. Braune, L. Bocklage, M. K. Czwalinna *et al.*, Sci. Adv. **8**, eabn6848 (2022).

[39] D. T. Matselyukh, V. Despré, N. V. Golubev, A. I. Kuleff, and H. J. Wörner, Nat. Phys. **18**, 1206 (2022).

[40] W. Hu, B. Gu, and I. Franco, J. Chem. Phys. **152**, 184305 (2020).

[41] M. A. Dugan, J. X. Tull, and W. S. Warren, J. Opt. Soc. Am. B **14**, 2348 (1997).

[42] A. M. Weiner, Rev. Sci. Instrum. **71**, 1929 (2000).

[43] M. Nisoli, S. De Silvestri, and O. Svelto, Appl. Phys. Lett. **68**, 2793 (1996).

[44] F. Hagemann, O. Gause, L. Wöste, and T. Siebert, Opt. Express **21**, 5536 (2013).

[45] A. Catanese, B. Kaufman, C. Cheng, E. Jones, M. G. Cohen, and T. Weinacht, OSA Continuum **4**, 3176 (2021).

[46] R. Trebino, K. W. DeLong, D. N. Fittinghoff, J. N. Sweetser, M. A. Krumbügel, B. A. Richman, and D. J. Kane, Rev. Sci. Instrum. **68**, 3277 (1997).

[47] I. Amat-Roldán, I. G. Cormack, P. Loza-Alvarez, E. J. Gualda, and D. Artigas, Opt. Express **12**, 1169 (2004).

[48] M. P. Fewell, Opt. Commun. **253**, 125 (2005).

[49] W. D. M. Lunden, P. Sándor, T. C. Weinacht, and T. Rozgonyi, Phys. Rev. A **89**, 053403 (2014).

[50] B. Kaufman, T. Rozgonyi, P. Marquetand, and T. Weinacht, Phys. Rev. A **102**, 063117 (2020).

[51] P. Sándor, V. Tagliamonti, A. Zhao, T. Rozgonyi, M. Ruckenbauer, P. Marquetand, and T. Weinacht, Phys. Rev. Lett. **116**, 063002 (2016).

[52] B. Kaufman, T. Rozgonyi, P. Marquetand, and T. Weinacht, Phys. Rev. A **103**, 023108 (2021).